SolarPACES 2024, 30th International Conference on Concentrating Solar Power, Thermal, and Chemical Energy Systems

Receivers and Heat Transfer Media and Transport: Point Focus Systems

https://doi.org/10.52825/solarpaces.v3i.2345

© Authors. This work is licensed under a Creative Commons Attribution 4.0 International License

Published: 22 Oct. 2025

# Numerical Prediction of the Initial Heating of Granular Material Treatment Using a Solar Rotary Kiln

#### SolarPaces 2024

Alessandro Gallo<sup>1,2,3,\*</sup> , Elisa Alonso<sup>3</sup> , and María Isabel Roldán Serrano<sup>4</sup>

 $^{\rm 1}$  Universidad Carlos III de Madrid, Thermal and Fluid Department, Spain

<sup>2</sup>Universidad de Almería, Spain

<sup>3</sup>Universidad Politécnica de Madrid, Spain

<sup>4</sup>German Aerospace Centre (DLR), Institute of Low-Carbon Industrial Processes, Germany

\*Correspondence: Alessandro Gallo, alessandro.gallo@upm.es, Elisa Alonso Romero elisa.alonso@upm.es

**Abstract.** Recent studies have proposed rotary kilns as solar receivers or reactors for industrial applications and for thermal storage. However, few investigations have focused on the temperature distribution within the particle bed, which is crucial for understanding system performance and developing optimization strategies. This work presents a comprehensive study of a lab-scale rotary kiln coupled with a high-flux solar simulator, examining the initial seconds of heating inert alumina spheres. Experimental data are compared and integrated with a two-dimensional thermo-fluid dynamic model using an Eulerian continuum approach. The model was initially validated for static particle heating and subsequently applied to simulate a rotating case, predicting temperature distribution in the transversal section of the granular bed. The results demonstrate the significant impact of rotation on homogenizing bed temperature and reducing thermal gradients. When the bed core reaches approximately 180°C, the maximum temperature difference between the center and sides is less than 50°C for the rotating configuration, compared to over 110°C for the static setup. This study provides valuable insights into the thermal behavior of rotary kilns as solar receivers, contributing to the optimization of their design and operation for various industrial and energy storage applications.

**Keywords:** Rotary Kiln, Concentrated Solar Energy, Thermal Energy Storage, Solar Heat for Industrial Process

#### 1. Introduction

Various traditional industrial sectors employ rotary kilns as reference equipment for heating processes. These devices can thermally treat materials of different size and shapes under different conditions. Among these materials, granular ones can be mixed at ambient temperature or heated to over 2000 °C. Depending on the specific process for which they are used, rotary drums function as dryers, heaters or chemical reactors [1]. Although rotary kilns have long been employed in the industrial sector, optimizing their performance and predicting both fluid-dynamic and thermal behavior for granular material treatments remain challenging. In the field of concentrated solar energy, rotary kilns have been studied at both laboratory and pilot scales. Several applications have been reported, including aluminum recycling, thermal and

thermochemical storage, solar fuels production, thermochemical water-splitting cycles, soil decontamination, and lime production, among others [1]. For instance, Neises et al. developed a solar-heated rotary kiln for thermochemical energy storage using cobalt oxide redox reactions [2]. Tescari et al. presented a large solar rotary kiln capable of heating particles to over 1000 °C at flow rates of up to 20 kg/h [3]. These advancements highlight the potential of solar rotary kilns for high-temperature industrial processes.

This paper aims to enhance the understanding of solar rotary kiln performance by applying CFD modeling using the Eulerian continuum approach by comparing it with experimental results obtained from a lab-scale rotary kiln built and tested at University of Antofagasta.

# 2. Experimental setup

A detailed description of the experimental setup is provided in a previous work by the authors of this study [4]. The main components are summarized below.

# 2.1 Rotary kiln

The University of Antofagasta rotary receiver (UARR) is a rotating cylindrical cavity that is insulated and enclosed in a static steel casing. An electric motor drives the rotor, allowing for speed variations. The kiln operates in batch mode, and during the experiment, its longitudinal axis was positioned horizontally. Before the beginning of the experimental test, thermocouple T1 was introduced into the cavity, shielded from radiation, and fixed to the inner wall (see Fig. 1a). The rotating thermocouple was connected to a wireless Data Acquisition System (DAQ), powered by an electric battery (see Fig. 2), and both rotated together with the kiln rotor. Thermocouples T2 and T3 were placed in different insulation layers. After particles were loaded, thermocouple T4 was introduced to measure the temperature inside the bed (see Fig. 1a). Fig. 1 shows the longitudinal and cross-sections of the UARR, along with main dimensions and thermocouple positions.

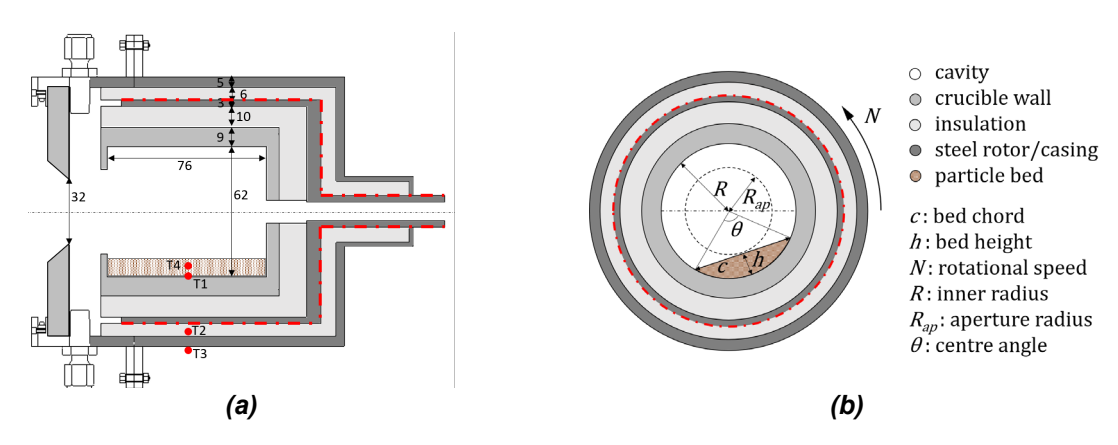


**Figure 1.** (a) Sketch of the rotary kiln longitudinal section. Lengths in millimeter. (b) Kiln transversal section. Red lines delimit inner rotating components from external static ones.

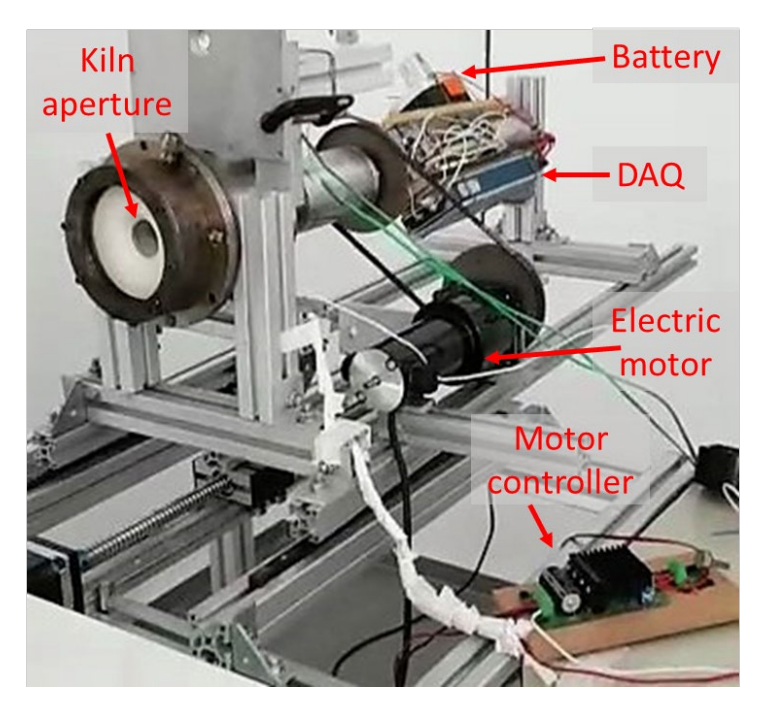


Figure 2. Experimental setup of the solar rotary kiln

#### 2.2. Solar simulator

The source of concentrated radiation used in the experimental tests was the Xenoluxe Lamphouse model of Proyecson, a 7-kW<sub>e</sub> high-flux solar simulator (HFSS) installed at Solar Concentration Laboratory of Antofagasta University (LaCoSA). Due to the high intensity of the radiation flux and the power at the focal plane, which could lead to steady-state temperatures higher than desired range (750 – 850 °C), the UARR aperture was positioned in a plane where the heat flux had a lower irradiance. A characterization of this simulator was performed in order to define the optimal position, resulting in an irradiance peak of approximately 800 kW·m<sup>-2</sup> and a power of 369 W inside a circumference of 32 mm in diameter [4].

# 3 Methodology

The experimental tests involved heating the empty rotating kiln with the HFSS until thermal steady state was reached. At that point, the lamp was turned off, the kiln cavity was filled with 45 g of 2-mm-diameter alumina spheres, and thermocouple T4 was introduced into the bed. Subsequently, the HFSS was turned on again, and the thermal steady state was reached once more. During the second heating, the cavity remained static to ensure accurate temperature measurements from T4.

Experimental data are complemented by insights derived from a Computational Fluid Dynamics (CFD) model, which is first validated under stationary conditions and then extended to include rotational dynamics, providing a comprehensive analysis of the system's behavior. Among the various CFD methodologies available, the Eulerian continuum approach (ECA) has gained prominence in modeling granular flows within rotary kilns. This method treats the granular phase as a continuous medium, allowing for efficient simulation of large-scale systems with high particle concentrations. By solving conservation equations for mass, momentum, and energy for both the gas and granular phases, the Eulerian approach can capture key phenomena such as particle-fluid interactions, heat transfer, and segregation effects [1]. For the calculations, the software Ansys Fluent 19.2 was employed in a computer with a 3.20 GHz processor and 16 GB RAM. 2D simulations were conducted with six parallel processors. Analyses of the transversal section of the kiln filled with 2-mm-diameter alumina spheres were satisfactorily carried out with a time step of 10-4 seconds. Both cases, with and without rotation, were

performed. At this stage of the investigation, due to the high computational demands, only the initial 16 seconds, corresponding to two kiln revolutions at a rotation speed of 7.5 rpm, were simulated. Several assumptions were made to simplify the problem:

- · No-slip walls
- · Alumina particles were spherical, rigid, and no cohesion was considered.
- The granular bed and the air were incompressible (constant densities).
- · Air viscosity was constant.
- Mass diffusion was negligible
- The coefficient of restitution was fixed at 0.9, representing a measure of the kinetic energy dissipated in a collision between particles. A value of 1 represents a perfect elastic collision.
- Normalized scaled residuals were set at 10<sup>-3</sup> for all the equations, except for radiation model, which was set at 10<sup>-6</sup>.
- The maximum iterations per time step were 40.
- A cell size of 0.4 mm, corresponding to 19,857 cells in the mesh, was selected according to the mesh independency study conducted.

The ECA treated the multiphase flow as a special fluid where the pressure is the same for both the gas (g) and solid (s) phases. In this analysis, the gas phase was air, and the alumina spheres represented the solid phase. Continuity and momentum equations were solved for both phases, and a balance of volume fraction ( $\alpha$ ) was applied ( $\alpha_g + \alpha_s = 1$ ). To calculate the solid pressure and the stress tensor for the solid phase, the kinetic theory of granular flow (KTGF) was included in the model. This theory draws an analogy with gas kinetic theory, where particles are compared to gas molecules with disordered movements and a Maxwellian velocity distribution. Therefore, a granular temperature  $(\theta_s)$  was defined as  $\theta_s = \frac{1}{3}\bar{c}_{sf}\bar{c}_{sf}$ . The bulk viscosity  $(\lambda_s)$  included in the stress tensor for the solid phase  $(\bar{\tau}_s)$  followed the formulation by Lun et al. [5], and the solid shear viscosity ( $\mu_s$ ) was considered as the sum of collisional, kinetic and frictional viscosity (see eq. 1). Syamlal et al. [6] expressions were used for the kinetic viscosity, collisional viscosity, the radial distribution function  $(g_{0,ss})$ , the diffusion coefficient of granular energy (see eq. 2), and momentum exchange between solid and fluid, while the Schaeffer model was employed for the frictional viscosity. The transport equation for the KTGF takes the form of eq. 3, where the terms of diffusion, collisional dissipation, and kinetic energy transfer follow are indicated in equations 2, 5, and 6, respectively. According to Tescari et al. [3], a laminar flow was used for air due to the low rotation speed of the kiln cavity.

$$\bar{\bar{\tau}}_s = \alpha_s \mu_s \left\{ \left[ \nabla \vec{v}_s + (\nabla \vec{v}_s)^T \right] + \alpha_s \left( \lambda_s - \frac{2}{3} \mu_s \right) \nabla \cdot \vec{v}_g I \right\}$$
 (1)

$$k_{\theta_s} = \frac{15 d_s \alpha_s \rho_s \sqrt{\theta_s \pi}}{4(41 - 33\eta)} \left[ 1 + \frac{12}{5} \eta^2 (4\eta - 3) \alpha_s g_{0,ss} + \frac{16}{5\pi} (41 - 33\eta) \eta \alpha_s g_{0,ss} \right] \text{ with } \eta =$$

$$\frac{1}{5} (1 + e_{ss})$$
(2)

$$\frac{3}{2} \left[ \frac{\partial}{\partial t} (\alpha_s \rho_s \, \theta_s) + \nabla \cdot (\alpha_s \rho_s \, \vec{v}_s \, \theta_s) \right] = \left( -p \bar{\bar{I}} + \bar{\bar{\tau}}_s \right) : \nabla \, \vec{v}_s + \nabla \cdot \left( k_{\theta_s} \nabla \theta_s \right) - \gamma_{\theta_s} + \varphi_{gs} \tag{3}$$

$$\gamma_{\theta_s} = \frac{12(1 - e_{ss}^2)g_{0,ss}}{d_s\sqrt{\pi}}\alpha_s^2 \rho_s \theta_s^{\frac{3}{2}}$$
 (5)

$$\varphi_{as} = -3K_{as}\theta_s \tag{6}$$

$$\frac{\partial}{\partial t}(\alpha_s \rho_s h_s) + \nabla \cdot (\alpha_s \rho_s \vec{v}_s h_s) = \alpha_s \frac{dp_s}{dt} + \bar{\tau}_s : \nabla \vec{v}_s - \nabla \cdot \vec{q}_s + Q_{gs}$$
 (7)

$$q_{rad} = -\Gamma \nabla G \tag{8}$$

$$\Gamma = \frac{1}{3(a + \sigma_s) - C\sigma_s} \tag{9}$$

$$\nabla \cdot (\Gamma \nabla G) = aG - 4an^2 \sigma T^4 + S_G \tag{10}$$

$$Nu_{s} = \left(7 - 10\alpha_{g} + 5\alpha_{g}^{2}\right)\left(1 + 0.7Re_{s}^{0.2}Pr^{\frac{1}{3}}\right) + \left(1.33 - 2.4\alpha_{g} + 1.2\alpha_{g}^{2}\right)Re_{s}^{0.2}Pr^{\frac{1}{3}}$$

$$\tag{11}$$

The conservation of energy was calculated using separate enthalpy equations for each phase. Eq. 7 represents the solid phase, where  $-\nabla \cdot \vec{q}_s$  includes convection, conduction, and radiative heat transfer (eq. 8-10). The P1 radiative model was used due to its compatibility with the ECA granular model and its suitability for optically thick media, such as granular materials in rotary kilns. The incident radiation (G) and its transport equation are defined by considering the weighted average attenuation coefficient of air and alumina. The radiation source ( $S_G$ ) corresponds to the crucible wall's radiation, with the alumina wall emissivity set to 0.07, assuming gray-surface behavior. Heat exchange between air and solids ( $Q_{gs}$ ) was calculated using the Gunn correlation (eq. 11), which is valid for specific porosity and Reynolds number ranges. Boundary conditions were split between the covered and uncovered parts of the crucible wall, with a combined heat transfer method applied to the uncovered part. Due to the complexity of heat flux balance during transient heating, a value of 25 kW m<sup>-2</sup> was selected to fit the experimental data. Material properties varying with temperature were incorporated into the model.

#### 3. Results

The 2D-CFD model provides insights into the motion of spheres and temperature distribution within the granular bed of the kiln. Significant differences in thermal and fluid-dynamic distribution appear between rotating and non-rotating cases.

The granular bed exhibits typical rolling behavior, with spheres reaching a maximum velocity of 0.20 m/s at the bed surface. No segregation occurs due to the uniform sphere size and low fill degree. The dynamic angle of repose (23° at the highest point, 8° at the lowest) aligns with experimental measurements and literature values (see Fig. 3b and 4) [7]. The volume fraction of the alumina spheres approaches the typical maximum limit of 0.63 for same-sized spheres, consistent with other models [8]. The air flow shows a counter flux in the central section (see Fig. 5), driven by sphere movement at the bed surface, and qualitatively agrees with previous research, although few studies report detailed information on this aspect [8].

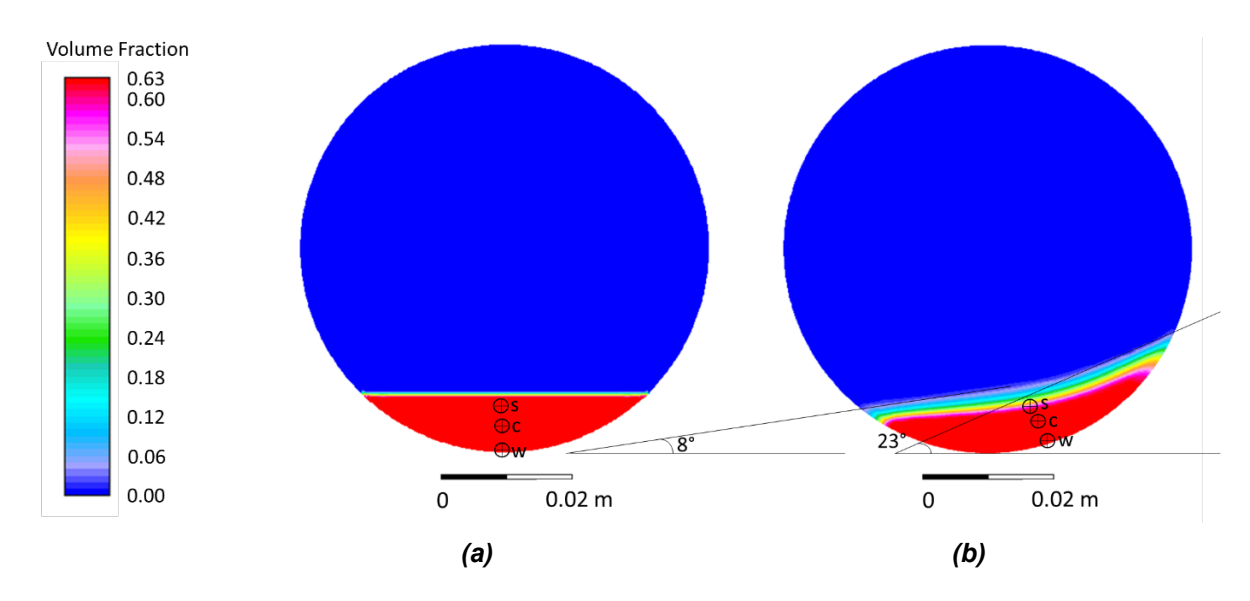


**Figure 3.** Volume fraction of alumina bed with selected points (s, c, and w) for temperature control. (a) Static bed and (b) rotating bed. Lowest and highest angles of the rotating bed are also indicated.

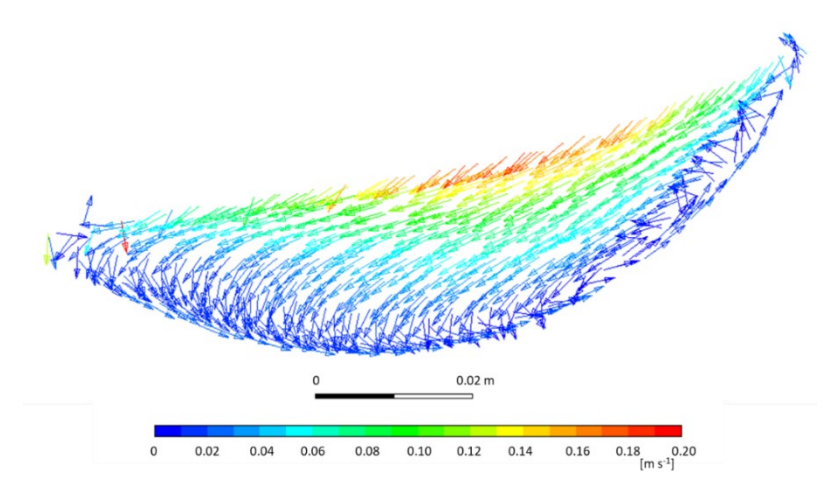


Figure 4. Speed of the alumina particles in the granular bed.

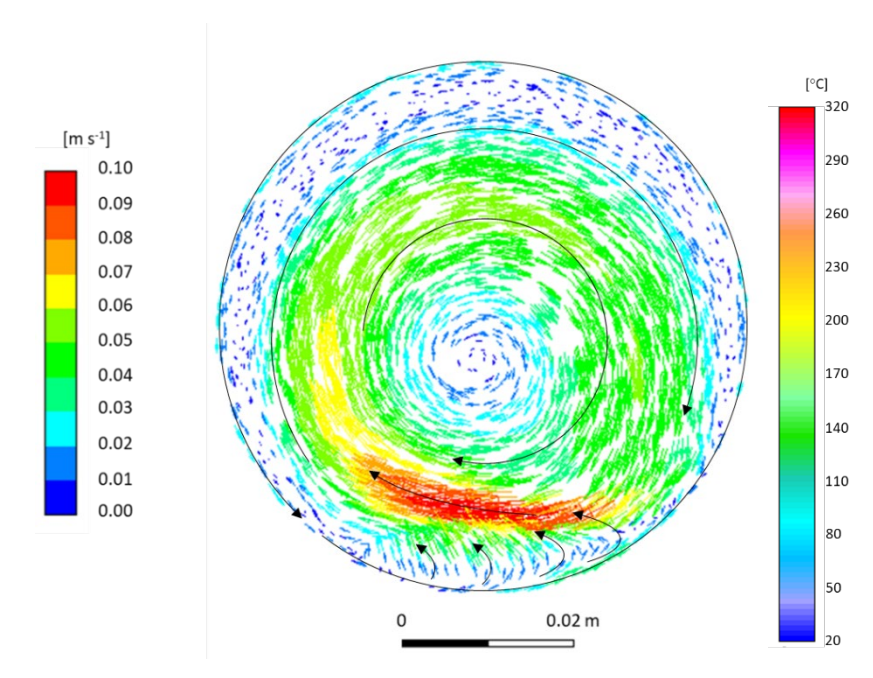
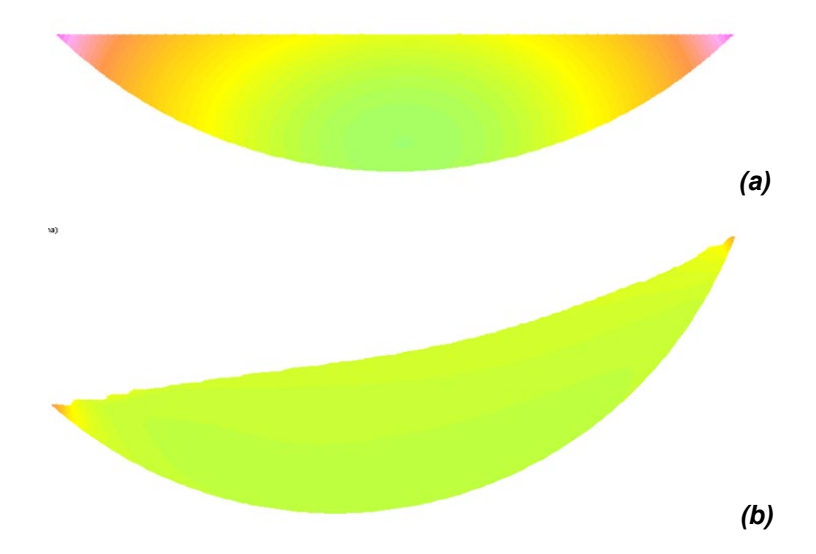
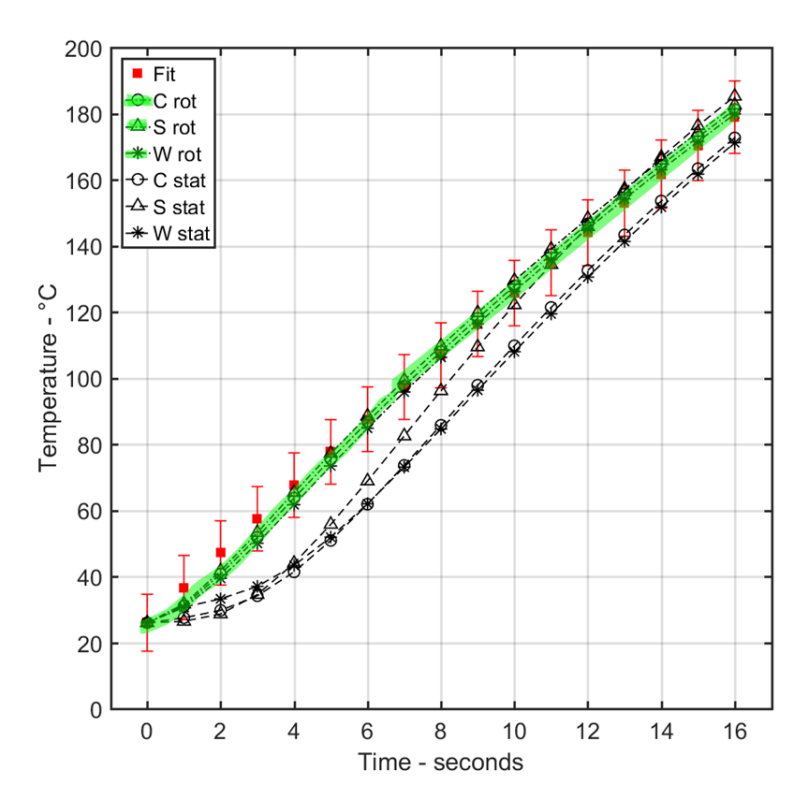


Figure 5. Air speed in the cross section of the UARR.



**Figure 6.** Temperature distribution in the particle bed after 16 seconds: (a) static bed, (b) rotating bed.



**Figure 7.** Comparison of temperatures in the middle (C), at the surface (S), and at the wall (W) for the rotating bed (rot) and static bed (stat) with the experimental data (Fit).

After 16 seconds, a maximum temperature difference of approximately 50 °C is estimated in the rotating bed, whereas more than 110 °C are observed in the static bed (see Fig. 6). Moreover, stratification in the core of the bed is avoided because spheres with the same diameter are used.

As shown in Fig. 7, the temperature extrapolated from experimental data shows a rapid increase from 0 to 180 °C in 16 seconds. This temperature profile is compared with the values obtained from simulations at different points defined in Fig. 3a and b as wall (w), center (c), and surface (s) for both static and rotating configurations. In both cases, temperature near the wall is the lowest, and at the surface, it is higher than in the core of the bed. However, when rotation is present, gradients of less than 4 °C appear, whereas in the static bed, gradients of approximately 15 °C are observed at the selected points.

Overall, the CFD model provides valuable insights into the kiln's thermal and fluid-dynamic behavior that experimental and one-dimensional analyses cannot capture. Thanks to CFD technique, solar receiver design and its control strategies can be enhanced through the optimization of parameters that promote more homogeneous mixing within the granular bed, leading to improved system efficiency.

#### 4. Conclusions

Although rotary kilns have been previously studied as solar receivers for the treatment of particles, a deep understanding of its temperature distribution remains a challenge. In this work, a combination of experimental and simulation analyses was performed to provide a more comprehensive understanding of the thermal behavior of solar rotary kilns. In particular, the results obtained from the CFD simulation contribute significantly to the assessment of the granular solid motion and temperature distribution within the bed. Kiln rotation promotes the homogenization of the temperature distribution and, in comparison with static beds, demonstrates that spheres movement reduces thermal gradients inside the bed and stratification is avoided. The

methodology proposed in this paper provides initial insights into particle heating in solar rotary receivers, which is fundamental for optimizing these devices, improves efficiency and enhances process control. Furthermore, results from this research will facilitate scalability of solar rotary receivers and boost their integration into industrial processes.

#### **Author contributions**

**A. Gallo:** Conceptualization, Data curation, Formal analysis, Investigation, Methodology, Software, Validation, Visualization, Writing – original draft. **E. Alonso:** Funding acquisition, Project administration, Resources, Supervision, Writing – review & editing. **M.I. Roldán-Serrano:** Supervision, Writing – review & editing.

# **Competing interests**

The authors declare that they have no competing interests.

# **Acknowledgement**

A. Gallo wishes to thank the University of Almería for his Margarita Salas post-doctoral fellow-ship RR\_A\_2021\_11 funded by the European Union within the framework of the "Recovery, Transformation and Resilience Plan" promoted by the Spanish government

#### References

- [1] E. Alonso, A. Gallo, M.I. Roldán, C.A. Pérez-Rábago, E. Fuentealba, "Use of rotary kilns for solar thermal applications: Review of developed studies and analysis of their potential", Sol. Energy. 144 (2017) 90–104. doi:10.1016/j.solener.2017.01.004
- [2] M. Neises, S. Tescari, L. de Oliveira, M. Roeb, C. Sattler, B. Wong, "Solar-heated rotary kiln for thermochemical energy storage", Sol. Energy, 86 (2012) 3040-48. doi: <a href="https://doi.org/10.1016/j.solener.2012.07.012">10.1016/j.solener.2012.07.012</a>
- [3] S. Tescari, M. Neises, L. de Oliveira, M. Roeb, C. Sattler, P. Neveu, "Thermal model for the optimization of a solar rotary kiln to be used as high temperature thermochemical reactor", Sol. Energy. 95 (2013) 279–289. doi:10.1016/j.solener.2013.06.021
- [4] A. Gallo, E. Alonso, C.A. Pérez-Rábago, E. Fuentealba, M.I. Roldán, "A lab-scale rotary kiln for thermal treatment of particulate materials under high concentrated solar radiation: Experimental assessment and transient numerical modeling", Sol. Energy, 188 (2019) 1013–1030. doi:10.1016/j.solener.2019.07.006
- [5] C.K.K. Lun, S.B. Savage, D.J. Jeffrey, N. Chepurniy, "Kinetic theories for granular flow: inelastic particles in Couette flow and slightly inelastic particles in a general flowfield", J. Fluid Mech. 140 (1984) 223. doi:10.1017/S0022112084000586.
- [6] M. Syamlal, W. Rogers, T.J. O'Brien, "MFIX documentation theory guide", 1993. doi:10.2172/10145548
- [7] Beakawi Al-Hashemi, H. M., Baghabra Al-Amoudi, O. S. "A review on the angle of repose of granular materials". Pow. Tec., 330, (2018) 397–417. doi.org/10.1016/j.pow-tec.2018.02.003
- [8] M.A. Delele, F. Weigler, G. Franke, J. Mellmann, "Studying the solids and fluid flow behavior in rotary drums based on a multiphase CFD model", Powder Technol. 292 (2016) 260–271. doi:10.1016/j.powtec.2016.01.026.